Journal of Geoscience and Environment Protection, 2025, 13(4), 159-185
https://www.scirp.org/journal/gep
ISSN Online: 2327-4344
ISSN Print: 2327-4336

Diagnosis of JJAS Flood/Drought Events and the Associated Atmospheric Circulation Anomalies over Ethiopia

Habtamu Tarekegn Negash[1,2*], Mulualem Abera Waza[1,2]

[1]State Key Laboratory of Climate System Prediction and Risk Management/Key Laboratory of Meteorological Disaster, Ministry of Education/Collaborative Innovation Center on Forecast and Evaluation of Meteorological Disasters, Nanjing University of Information Science and Technology, Nanjing, China
[2]Ethiopian Meteorological Institute (EMI), Addis Ababa, Ethiopia
Email: *yehabtamug2009@gmail.com

How to cite this paper: Negash, H. T., & Waza, M. A. (2025). Diagnosis of JJAS Flood/Drought Events and the Associated Atmospheric Circulation Anomalies over Ethiopia. *Journal of Geoscience and Environment Protection, 13,* 159-185.
https://doi.org/10.4236/gep.2025.134009

Received: March 18, 2025
Accepted: April 13, 2025
Published: April 16, 2025

Abstract

Understanding the major drivers of Ethiopian JJAS rainfall variability is crucial for monitoring climate extremes such as drought and flood events, which have serious implications for lives, livelihoods and food security. This study investigates the atmospheric and oceanic mechanisms that modulate JJAS rainfall using composite analysis, probability evaluation of the Z-index, and correlation analysis with leading climate drivers, including sea surface temperatures (SSTs), wind circulation, and outgoing longwave radiation (OLR). The results show that 40.3% of JJAS rainfall is normal, 29.5% and 30.2% are dry and wet, respectively. Wet years have sharply increased since 1998, showing a shift in the rainfall patterns. Wind circulation analysis shows that 850 hPa westerly and 200 hPa easterly winds occur during wet years, which enhance the transport of moisture and convection, whereas dry years have their wind patterns in reverse, suppressing rainfall. The correlation of Sea Surface Temperature with rainfall in JJAS has a very significant negative correlation (−0.8) in central and eastern Pacific SSTs, indicating La Niña enhancing rainfall and El Niño deficit it. Conversely, a significant positive correlation (0.8) in the western Pacific modulating the regional SST anomaly Ethiopian rainfall. The Nino 3.4 Index shows a significant negative relationship (−0.5 to −0.8) with Ethiopia's JJAS rain, especially in the northeast, central, and eastern regions, the key role of the ENSO in rainfall variability. Moreover, the negative OLR anomaly and high RH, promote cloudiness and precipitation, while dry years are distinguished by the higher OLR anomaly and reduced RH, which suppress convection. These results confirm the leading influence of the El Nino-Southern Oscillation (ENSO) in controlling Ethiopian rainfall variability and suggest that monitor-

ing of SST structure, particularly the Nino 3.4 Index, might enhance seasonal rainfall prediction and inform the Ethiopian climatic change strategy. Future studies should incorporate high-resolution modeling, improved observations, advanced statistics, and Machine Learning to better comprehend Ethiopia's climate extremes.

Keywords

ENSO, Ethiopian Rainfall Variability, Flood and Drought, JJAS Precipitation, Sea Surface Temperature Anomalies, Wind Circulation Patterns

1. Introduction

Ethiopia faces significant challenges from climate extremes, including drought and floods, which affect people's life, livelihood, and food security (Climate Risk Profile, n.d.; OCHA, 2024; UNISDR, 2015). Rainfed agriculture, which contributes roughly 40% of GDP, 80% of jobs, and 90% of exports, is crucial to Ethiopia's food security and economy (Diao et al., 2023; FAO, 2016; MoEF (Ministry of Environment and Forest), 2015). Nonetheless, the importance of this sector makes the country more vulnerable to weather-related risks, with the potential of yearly average GDP losses of 1% - 1.5% (World Bank Group, 2024), and possibly increasing to 8% - 10% by 2050 (CIAT, BFS/USAID, 2017).

Rainfall is the most significant climatic element for the socio-economic development of Ethiopia (Cheung et al., 2008; Conway & Schipper, 2011). Rainfall patterns of the country show substantial spatial and temporal variability, which are highly influenced by the diversity of the topography and latitudinal range of the country (Gamachu, 1988). Spatially, rainfall amount, seasonal cycles, onset and cessation times, and growing season lengths are highly variable across Ethiopia due to its diverse topography and complex climatic mechanisms (Gamachu, 1988; Segele & Lamb, 2005). The highlands have longer growing seasons and higher rainfall while the lowlands are arid and have minimal and erratic precipitation (CONWAY, 2000; Deressa et al., 2009). Such variability poses significant challenges to agricultural planning and food security because the variability in rainfall patterns has a direct influence on crop production and water availability (Bewket & Conway, 2007; Seleshi & Zanke, 2004).

The amount and direction of Ethiopia's rainfall varies temporally, ranging from daily to decadal patterns in different locations and seasons (Cheung et al., 2008; Degefu et al., 2017; Jury & Funk, 2013; Seleshi & Zanke, 2004). According to (Gummadi et al., 2017), rainfall also shows greater temporal variability, with a coefficient of variation that ranges from 9% - 30% annually during Kiremt seasons and 15% - 55% during Belg seasons. Ethiopia's complex spatiotemporal rainfall variability is primarily driven by variations in altitude (Gamachu,1988), sea surface temperature across the Pacific, Indian, and Atlantic Oceans (Degefu et al., 2017; Korecha & Barnston, 2007; Segele et al., 2009; Viste & Sorteberg, 2013), cou-

pled with inter-seasonal and interannual variations in the Arabian Peninsula monsoon intensity (Segele et al., 2009). The meridional migration of the Inter-Tropical Convergence Zone (ITCZ) across Ethiopia's complex topography regulates the seasonal rainfall cycle (Kassahun, 1987; Segele & Lamb, 2005).

A number of studies have been carried out on the drivers of rainfall variability in Ethiopia, with a focus on the predictability of June to September rainfall and the link between equatorial eastern Pacific sea surface temperature and Ethiopian rainfall across all seasons (Degefu et al., 2017; Alhamshry et al., 2019; Diro et al., 2011; Gissila et al., 2004; Korecha & Barnston, 2007; Segele et al., 2009; Seleshi & Zanke, 2004). Research has shown that ENSO has a significant impact on the Ethiopian rainfall pattern, with El Nino conditions often resulting in drought and La Nina conditions in excess rainfall and flooding (Abdi et al., 2016; Degefu et al., 2017; Gobie & Miheretu, 2021; Korecha & Barnston, 2007; Mulualem Abera & Wen, 2021; Segele & Lamb, 2005; Seleshi & Zanke, 2004). Moreover, the study established that a stronger TEJ leads to an increase in rainfall and short dry spells, while a weaker TEJ results in a decrease in rainfall and long dry spells in the summer (Diro et al., 2015; Segele & Lamb, 2005).

Although there has been extensive climate research in Ethiopia, few studies (Diro et al., 2015; Nicholson, 2017; Segele et al., 2009) have been carried out to characterize rainfall features and their association with atmospheric circulation, which is vital for seasonal and long-term climate prediction. In the same manner, while there are works (Berihu et al., 2024) on the variability of rainfall in southern and southeastern Ethiopia during MAM season, there is still a gap in understanding how changes in the atmospheric circulation affect rainfall patterns, particularly drought and flood events, during the JJAS season. Therefore, this study aims to fill this gap by investigating significant drought and flood events during Ethiopia's Kiremt (June-September) season and the associated atmospheric circulation anomalies. The research will identify the major flood/drought occurrences in recent decades and examine how atmospheric circulation anomalies influence these extreme events. Applying advanced approaches and long-term data, this study will give insight into the prediction of extreme events and thus enhance disaster preparedness and climate change adaptation strategies in Ethiopia.

This paper continues as follows. Section 2 shows the study area, data, and methods; Section 3 presents and discusses the results; Section 4 summarizes and concludes the main findings.

2. Study Area, Data and Methods

2.1. Study Area

Ethiopia, which lies within the Horn of Africa between latitudes 3˚ N to 15˚ N and longitudes 33˚ E to 48˚ E (**Figure 1**), has an area of more than 1.1 million square kilometers and is bordered by Eritrea in the north, Djibouti in the northeast, Somalia in the east and southeast, Kenya in the south, and Sudan and South Sudan in the west. Ethiopia's topographical diversity features high mountains, flat topped

plateaus, and lowlands; with altitudes ranging from 126 m below sea level in the Danakil Depression to over 4600 m in the Simien Mountains (MoEF (Ministry of Environment and Forest), 2015). The variation contributes to the complex climatic variability, ranging from humid equatorial rainforest to semi-arid and desert conditions (MoEF (Ministry of Environment and Forest), 2015).

Ethiopia's climate and seasonal rainfall are modulated by its complex topography and the migratory patterns of Inter-Tropical Convergence Zone (ITCZ), showing significant interannual variability. Mean annual temperature varies from less than 15˚C in the highlands to above 25˚C in the lowlands (FAO, 2016; MoEF (Ministry of Environment and Forest), 2015). The mean annual rainfall in Ethiopia is highly variable, with more than 2000 mm in the southwest-northwest sectors, but less than 300 mm in the southeast and northeast lowlands (Climate Risk Profile, n.d.; FAO, 2016; MoEF (Ministry of Environment and Forest), 2015). Generally, rainfall is higher over the highlands than the lowlands (Diro et al., 2011).

The ITCZ oscillates across the equator, reaching its northernmost position at 15˚ N over northern Ethiopia in July and its southernmost at 15˚ S in January (MoEF (Ministry of Environment and Forest), 2015; Nicholson, 2018; Segele & Lamb, 2005; Segele et al., 2009). Ethiopia experiences three different rainy seasons. They are Bega which occurs in October to January, Belg which occurs in February to May, and Kiremt which spans from June to September (Gissila et al., 2004; Korecha & Barnston, 2007; Segele & Lamb, 2005). Kiremt is the main rainy season, it aligns with the ITCZ's northernmost position, and accounts for 50% - 80% of annual rainfall. Northern and central Ethiopia also experience a secondary wet season, Belg; characterized by sporadic and lesser rainfall. Southern and southeastern Ethiopia experience two distinct wet seasons as the ITCZ passes through: Belg, the main rainy season, and Bega, which features lower rainfall for the region and also cooler temperatures in Ethiopia.

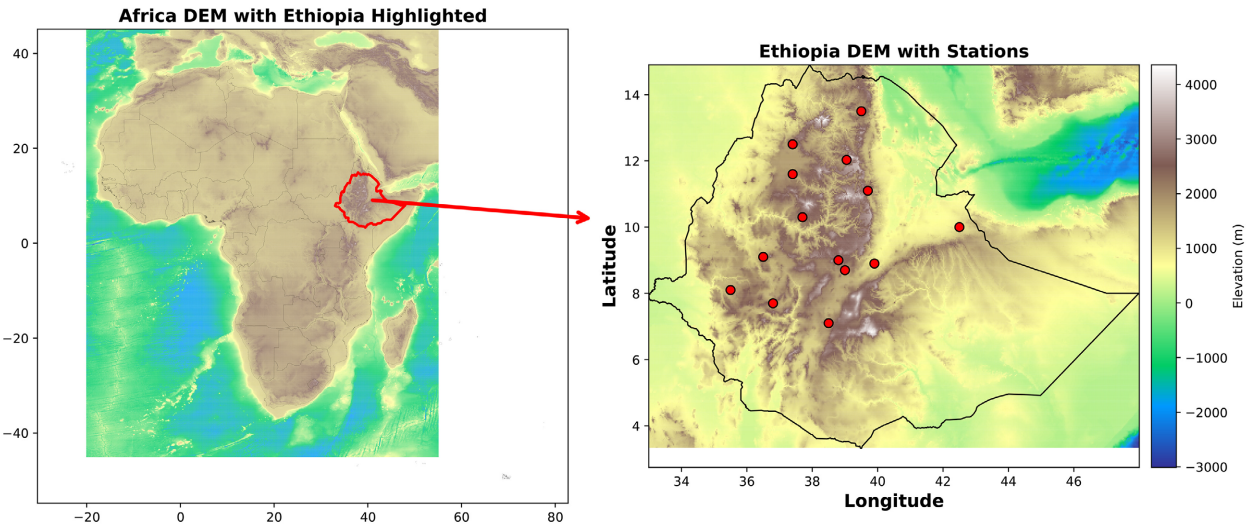

Figure 1. Geographical location and Topographical map of Study area, Ethiopia in Meter with stations distribution (red dots represent stations distribution).

During Belg season, northward advance of ITCZ results in orographic rains in southwestern and southcentral Ethiopia. This happens because moist air flows from Indian Ocean and Gulf of Aden largely through low pressure systems over South Sudan (Segele et al., 2009; Viste & Sorteberg, 2013). Also, meridional arm of ITCZ enhances rainfall in southwestern Ethiopia. This is due to heat capacity differences between the land surface and the Indian Ocean (Kassahun, 1987). During Kiremt, ITCZ reaches its northernmost position. This leads to significant moisture influx across Ethiopia. It is driven by westerly winds transporting moisture from the Atlantic and Indian Oceans, which result in widespread rains (MoEF (Ministry of Environment and Forest), 2015; Segele et al., 2009). Following the seasonal retreat of ITCZ in September, light rains can be experienced in southern Ethiopia until November. However, dry Bega season is characterized by dry and cool conditions in Ethiopia. This is because northeasterly winds dominate the region, and also ITCZ remains positioned south of Ethiopia. Variability in Indian Ocean sea surface temperature affects the cyclical movement of ITCZ. This leads to significant interannual fluctuation in onset and duration of rainfall seasons. Topographic variations further complicate the distribution of rainfall.

2.2. Data

The study uses monthly rainfall records at 14 synoptic stations in Ethiopia, sourced from the Ethiopian Meteorology Institute to identify notable drought and flood years from 1981 to 2022. The climatological mean of the period was used for analyzing anomalies. Besides, gridded precipitation data were also obtained from Climate Hazards Group InfraRed Precipitation with Station data (CHIRPS) version 2 (Funk et al., 2015) was used to analysis of spatial rainfall patterns and extreme climate events. This invaluable dataset was developed by the Climate Hazards Group at the University of California, Santa Barbara (UCSB) in collaboration with United States Geological Survey (USGS), offers extensive temporal coverage, open access, and high spatial resolution ($0.05^\circ \times 0.05^\circ$). It has been validated in numerous studies to show lower biases and outperformed than other satellite-based rainfall products such as ARC2 and TAMSAT (Ayehu et al., 2018; Dinku et al., 2018, Ngoma et al., 2021). The data available at:
https://data.chc.ucsb.edu/products/CHIRPS-2.0/global_monthly/netcdf/.

The study used NCEP/NCAR reanalysis atmospheric data sets, which include monthly mean zonal and meridional winds, vertical velocity (omega), velocity potential, and relative humidity, all at a resolution of $2.5^\circ \times 2.5^\circ$ (Kalnay et al., 1996; Kistler et al., 2001). These datasets have previously been used for analyzing large-scale atmospheric circulation in Ethiopia (Segele et al., 2009) and are freely accessible at:
https://iridl.ldeo.columbia.edu/SOURCES/.NOAA/.NCEP-NCAR/.CDAS-1/.MONTHLY/.Intrinsic/.PressureLevel/

The study utilized monthly global sea surface temperature (SST) data from the Extended Reconstructed Sea Surface Temperature (ERSSTv5), developed by the

National Oceanic and Atmospheric Administration's National Centers for Environmental Information (NOAA/NCEI) (Huang et al., 2017). This dataset is at spatial resolution of 2˚ × 2˚ and is freely accessible at: https://iridl.ldeo.columbia.edu/SOURCES/.NOAA/.NCDC/.ERSST/.version5/.sst/. Moreover, the study also applied global Outgoing Longwave radiation (OLR) data obtained from the National Oceanic and Atmospheric Administration (NOAA) Physical Science Laboratory (PSL) in Boulder, Colorado, USA. These data are available at a spatial resolution of 2˚ × 2˚ and can be accessed freely from the PSL website: https://psl.noaa.gov/data/gridded/data.olrcdr.interp.html.

2.3. Methods

2.3.1. China Z Index (CZI) for Grading Severity of Droughts and Floods

There have been numerous drought indices and methods developed during the past years that are now being applied worldwide to assess and monitor drought and flood conditions. Among others, these are the Palmer Drought Severity Index (PDSI) (Dai, 2011), Standardized Precipitation Index (SPI) (Dogan et al., 2012), Standardized Precipitation Evaporation Index (SPEI) (Dong et al., 2023), and the China Z Index (CZI), utilized in this study, was first developed in 1995 by the National Climate Center of China for assessing and monitoring drought and flood events (Wu et al., 2001).

In this study, the China Z Index (CZI) has been chosen to grade drought and flood events, assuming that monthly precipitation obeys Pearson type III distribution (Wang et al., 2003). This is because due to its comprehensive approach, which includes regional wet and dry indices and a severity grading scheme as proposed by Tan et al. (2003), the indices highlight different grade influences and acknowledge how the normal grade affects regional severity. Additionally, it has seen limited application in Ethiopia, a country with data scarcity, making its effectiveness in capturing regional drought flood events less explored. Comparative analyses have confirmed that the Z-Index performs similarly to other indices like the SPI and Z-score while being simpler to calculate and allowing missing data, making it useful for regions facing data scarcity, even though it has limitations due to lack of distribution fitting to gamma or Pearson type III distribution, shorter timescales may be less well represented compared with SPI (Wu et al., 2001). How ever we acknowledge its limitations and have addressed them by discussing its constraints, justifying its use, and suggesting future comparisons with other indices.

Many studies have successfully used the Z-Index for the analysis of drought and flooding phenomena in different locations. For example, Tan et al. (2003) used the Z-Index to study flood and drought events occurring in North China, while Dogan et al. (2012) who confirmed by validated the index as consistent for evaluating multi-monthly rainfall-based drought-induced severity in a semi-arid region of Turkey. Additionally, Suribabu & Sujatha (2019) used this index for classifying antecedent moisture levels in Coonoor station in India. The work of Ogwang et al. (2012) also applies the Z-Index to the analysis of the flood and drought events that occurred in Uganda from September to November. Similarly, Alexander &

Nyasulu (2021) applied the Z-Index to diagnose wet and dry events and their atmospheric circulation anomalies in Malawi, southeastern Africa. Therefore, the Z-Index, enhanced by a set of new regional flood/drought indices and grading schemes proposed by Tan et al. (2003), is effectively employed in this study.

The single Z-index is used to grade the severity of drought and flood events at each station in the study area, as described in Equation (1):

$$Z_i = \frac{6}{C_s}\left(\frac{C_S}{2}\varnothing_1 + 1\right)^{1/3} - \frac{6}{C_s} + \frac{C_s}{6} \tag{1}$$

where C_s and $\varnothing_i$ are the skewness coefficient and normalized variables, respectively, and they are described as;

$$C_s = \frac{\sum_{i=1}^{n}\left(x_i - \overline{x}\right)^3}{n\sigma^3}, \varnothing_1 = \frac{x_i - \overline{x}}{\sigma} \tag{2}$$

The climatological mean $\overline{x}$ and standard variance σ are defined as:

$$\overline{x} = \frac{1}{n}\sum_{i=1}^{n} x_i, \sigma = \sqrt{\frac{1}{n}\sum_{i=1}^{n}\left(x_i - \overline{x}\right)^2} \tag{3}$$

where x_i denotes the unprocessed variable.

Conversely, the severity of drought and flood events across the entire study area is evaluated in the context of the regional indices, as illustrated below:

$$I_F = \frac{\left(\sum_{i=1}^{3} n_i/P_i + n_4^+/P_4\right)}{n}, I_D = \frac{\left(\sum_{i=5}^{7} n_i/P_i + n_4^-/P_4\right)}{n} \tag{4}$$

The expressions (4) give the flood index, I_F and the drought index I_D, where P_i denotes the probability of grade i, P_4 is the same as P_i but for grade 4, n_i is the total station number of grade i, n_4^- is the same as n_i but for grade 4 with the negative anomaly, n_4^+ is similar for grade 4 but for normal grade with the positive anomaly. The new indices are established on the principle that a single station's contribution to regional flood or drought severity is directly proportional to its statistical probability; thus, stations with lower statistical probabilities significantly impact regional extreme events (Tan et al., 2003).

From expression (4), it is evident that the indices highlight the different impacts of varied grades while also acknowledging how the normal grade influences regional severity. They can objectively identify the intensity and degree of the affected areas (Tan et al., 2003). The seven grades and corresponding standards listed in **Table 1** include extreme flood, severe flood, mild flood, normal, mild drought, severe drought, and extreme drought.

Table 1. Standards for grading drought and flood using the single Z index and the regional index.

No.	Grades	Z index	Theoretical probability	Regional Index
1	Extreme Flood	$Z \geq 1.645$	5%	$I_F - I_D \geq 1/P_2$
2	Severe Flood	$1.0367 \leq Z < 1.645$	10%	$1/P_3 \leq I_F - I_D < 1/P_2$

Continued

3	Mild Flood	$0.5244 < Z < 1.0367$)	15%	$1/P_4 < I_F - I_D < 1/P_3$
4	Normal	$-0.5244 \le Z \le 0.5244$)	40%	$-1/P_4 \le I_F - I_D \le 1/P_4$
5	Mild Drought	$-1.0367 < Z < -0.5244$	15%	$-1/P_5 \le I_F - I_D < 1/P_4$
6	Severe Drought	$-1.645 < Z \le -1.0367$	10%	$-1/P_6 < I_F - I_D \le 1/P_5$
7	Extreme Drought	$Z \le -1.645$	5%	$I_F - I_D \le 1/P_6$

2.3.2. Composite Analysis

Composite mean analysis method is employed in this study to examine the circulation anomalies associated with wet and dry events. Composite analysis is a method that involves identifying and averaging a single or more categories of variable, typically selected based on their association with key conditions (Folland, 1983). The results from this analysis are often used to develop hypothesis about patterns that may be associated with particular scenarios, this analysis assists in understanding complex atmospheric phenomena. It is most valuable to increase understandings of the relationships between different climate variables and extreme events, providing valuable insights for further investigation. In this study, the composite analysis for dry and wet years was conducted separately to focus on detecting circulation anomalies related to droughts and floods (the key conditions), utilizing ocean-atmospheric variables such as wind, vertical velocity (omega), velocity potential, outgoing longwave radiation (OLR), and relative humidity. This method has been widely applied by several authors, including Ogwang et al. (2012), Alexander & Nyasulu (2021) and Berihu et al. (2024), demonstrating significant atmospheric influence on drought and flood event. The composite mean analysis of atmospheric variables for dry and wet year's statistically significance is tested by using the student's t-test method which is described in (Equation (5)).

2.3.3. Student's t-Test (Difference of Mean)

The student's t-test is a technique to investigate whether there exist distinguishable differences between two sample means, accounting for their variability due to sampling (Wilks, 2011). For example, suppose precipitation data were being interpreted. In that case, the sample mean calculated from observations at station (A) may differ from actual/true population mean due to random variability of sampling. In climate studies, the null hypothesis states that the selected composite means (for specific climatic events and circulation pattern) do not significantly differ from the long-term climatological means of the entire dataset (Von Storch & Zwiers, 1984). This null hypothesis is rejected if the probability (p-value) of observing the mean difference by random chance is less than 0.05, which means statistical significance.

$$t = \frac{\overline{x}_1 - \overline{x}_2}{\sqrt{\left(\frac{(n_1-1)s_1^2 + (n_2-1)s_2^2}{n_1+n_2-2}\right)\left(\frac{1}{n_1}+\frac{1}{n_2}\right)}} \tag{5}$$

where $\overline{x}_1$ and $\overline{x}_2$ are the sample mean of group 1 and group 2, n_1 and n_2 are the corresponding sample size of group 1 and group, S_1 and S_2 denotes the sam-

ple standard deviations of group 1 and group 2, respectively. In this study, the mean JJAS seasonal anomalies were computed for both wet and dry events and then tested for statistical significance at a 95% confidence level for each case individually.

2.3.4. Correlation Analysis

Correlation is a statistical measure used to indicate the strength and direction of a relationship between two variables. To understand the air-sea interaction correlation analysis is employed in this study. This method shows the simple relationship between pairs of variables (Wilks, 2006; Wilks, 2011). In this study, correlation analysis is used to assess whether there are some significant relationships between climatic factors and rainfall like JJAS seasonal rainfall, how ENSO extremes (El Nino and La Nina) and JJAS seasonal rainfall are related, and their association with drought and flood events over the study area.

The simple correlation (r_{xy}) between variables X and Y may be expressed as:

$$r_{xy} = \frac{\sum_{i=1}^{n}\left(x_i - \overline{x}\right)\left(y_i - \overline{y}\right)}{\sqrt{\sum_{i=1}^{n}\left(x_i - \overline{x}\right)^2}\sqrt{\sum_{i=1}^{n}\left(y_i - \overline{y}\right)^2}} \tag{6}$$

where n is equal to the number of pair's scores; r_{xy} is the correlation coefficient; x_i is the values of the x-variable in a sample; $\overline{x}$ is mean of the values of the *x*-variable; y_i is values of the y-variable in a sample; and $\overline{y}$ is mean of the values of *y*-variable.

It calculates the degree of correlation between changes in one variable and changes in another. The simple correlation coefficient $\left(r_{xy}\right)$ has two important properties, the first one is its values should range from −1 to +1, and second, when the value of $\left(r_{xy}\right)$ is +1 or −1, it shows a strong positive or negative correlation between the given pairs of variables, respectively and if the values of $\left(r_{xy}\right)$ are 0, no correlation between two variables (independent variable). The square of the correlation coefficient $\left(r_{xy}\right)$ represents the portion of the variability of one of the two variables that is linearly accounted for or explained by the other. This method is used by several authors (Ogwang et al., 2012; Makula & Zhou, 2021). The calculated correlation coefficients were tested for statically significance using the t-test, and defined as:

$$t = r_{xy}\sqrt{\left(N-2\right)/\left(1-r_{xy}^2\right)} \tag{7}$$

The calculated values of t were then compared with those of the theoretical t-distribution with $N-2$ degrees of freedom. If the calculated value of t is greater or equals to the theoretical value, then the correlation is significant. A significant correlation in two or more variables indicates the predictive potential (Wilks, 2006).

3. Results and Discussions

3.1. JJAS Seasonal Rainfall Climatology for Stations

Figure 2 shows the JJAS (June-September) seasonal rainfall climatology of various

meteorological stations in Ethiopia, illustrating distinct spatial variations in regimes of precipitation. Among the stations, Nekemte experiences the most seasonally concentrated rainfall of more than 1400 mm, implying its location within a very moist and convective area. Bahir Dar and Gore also receive considerable rainfall totals of more than 1000 mm, indicating their proximity to large bodies of water and orographic enhancement that favors precipitation. Debre Markos, Gondar, and Jimma have moderately high rainfall, 800 - 1100 mm, reflecting the wettest nature of their highland regions. Addis Ababa, the capital city, receives about 700 - 800 mm of rainfall, which reflects a balance between moderate topographic relief and moist advection from neighboring systems. Hawassa receives less rainfall at about 500 mm, reflecting the relatively dry character of the Rift Valley environment. Locations such as Debre Zeit, Lalibela, Kombolcha, and Mekele experience intermediate levels of precipitation of between 500 and 700 mm, with the impact of altitude and localized atmospheric circulation patterns. Dire Dawa and Metehara, on the other hand, experience significantly lower precipitation, below 400 mm, indicating the arid to semi-arid nature of the lowlands in the eastern and rift valley areas. The significant differences between JJAS rainfall totals at these stations emphasize the complex interplay of topography, atmospheric circulation, and the proximity to water sources that all collectively control Ethiopia's seasonal pattern of rainfall. Knowledge of such patterns is essential for agricultural planning, water resources management, and climate adaptation policies in regions across the country.

3.2. Annual Rainfall Cycle and Anomaly Areal Average

The patterns of the annual rainfall cycle over Ethiopia are presented in **Figure 3(a)**, based on three data sets including, observed (gauge), CHIRPS, and CRU reanalysis data. It can be observed that the JJAS (Kiremt) season is the main rainfall season for Ethiopia, while the FMAM (Belg) season is the second wet season, and the ONDJ (Bega) period is relatively dry. The JJAS interannual rainfall variability, based on the standardized rainfall anomaly (SRA), is illustrated in **Figure 3(b)**. We can see that there were more dry years than wet periods before 1998, with 13 dry events and 4 wet events. While, after 1998, the frequency of wet events increased compared to dry events. Furthermore, the figure shows consecutive dry and wet years, notably from 1982 to 1987 and from 2017 to 2022, respectively.

3.3. Diagnosis of Flood and Drought Events

Table 2 presents the probability of flood/drought events for individual stations based on the single Z index, and shows consistency of calculated drought and flood frequency distribution with the theoretical probability provided in **Table 1**. The normal grade accounts for 40.3%, which is nearly equal to the theoretical standard of 40%. Severe floods make up 9.0%, and mild floods account for 16.1%, both slightly differing from the theoretical equivalent of 10% and 15%, respectively. Overall, around 40.3% of recorded rainfall is classified as normal, while 29.5% represents dry conditions and 30.2% accounts for wet conditions.

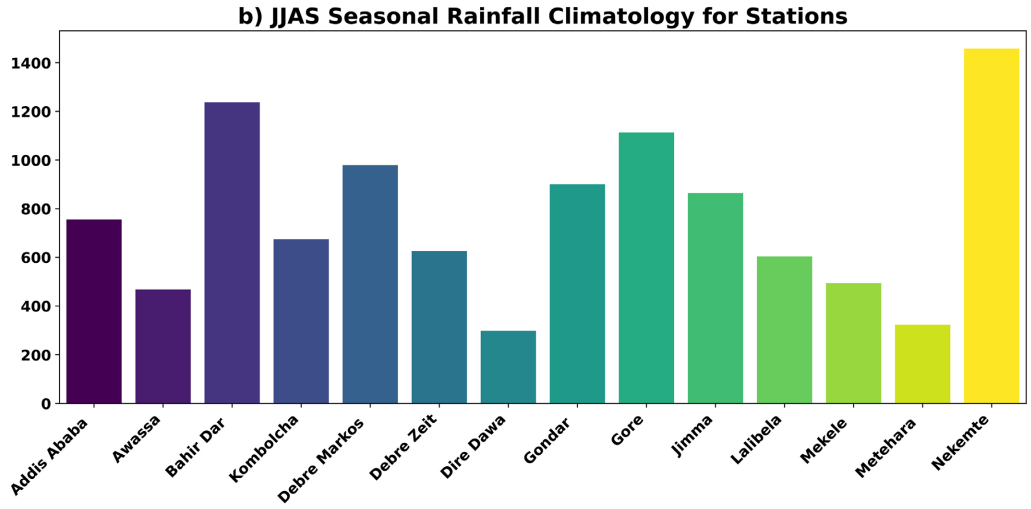

Figure 2. Stations used in this study with their JJAS seasonal rainfall climatology in millimeters.

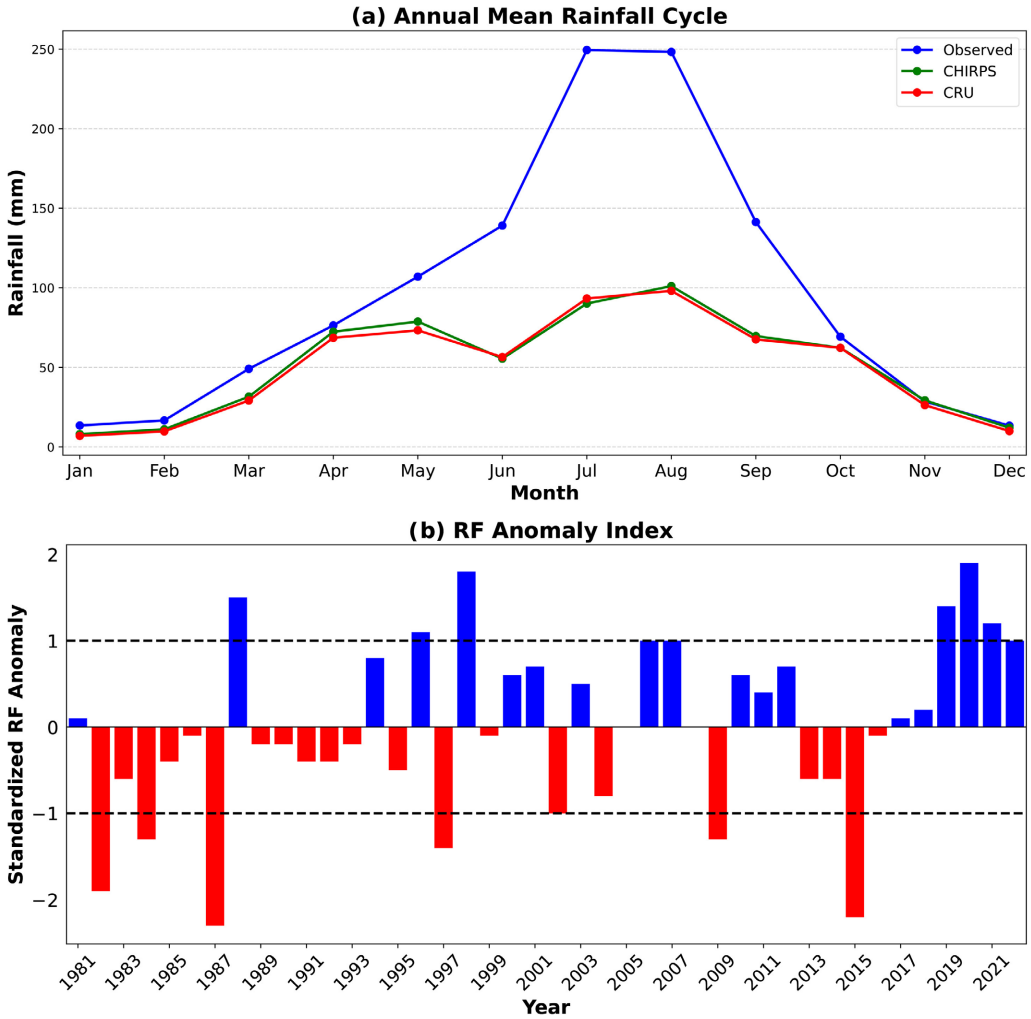

Figure 3. Annual mean rainfall cycle in temporal analysis, Observed, CHIRPS, and CRU data set in the top panel (a), and (b) JJAS seasonal rainfall Anomaly for areal average based on Observed data set in the bottom panel.

Table 3 shows the result of regional flood and drought years, in which the actual probability is highly correlated with the single theoretical probability of each grade. Notably, in 1988 and 2020, there were extreme floods, while in 1996, 1998, 2007, and 2019, there were severe floods. Contrary to this, in 1982, 1987, and 2015, there were extreme droughts, while in 1984, 1997, and 2009, there were severe droughts, which aligns with previous study (Viste et al., 2013). There were 14 wet years out of 42 years, comprising extreme, severe, and mild floods, while there were 12 dry years out of 42 years, comprising extreme, severe, and mild droughts. The numbers of wet and dry years in Table 3 are consistent with JJAS standardized rainfall anomaly presented in Figure 3(b), regarding the occurrence and frequency of these events. Moreover, it is evident that dry events slightly dominated before 1998, accounting for 7 out of 12 years, whereas wet events became prevalent from 1998, accounting for 11 out of 14 years.

Table 2. Years and probability of droughts and floods at 14 stations using a single Z index.

Stations/ Grades	Extreme Flood	Severe Flood	Mild Flood	Normal	Mild Drought	Severe Drought	Extreme Drought
AA	3	2	5	24	5	1	2
AW	2	5	6	17	5	6	1
BDR	2	5	5	20	4	3	3
COB	2	4	7	18	5	4	2
DD	3	3	6	19	4	5	2
DM	2	4	6	17	6	5	2
DZ	2	6	5	16	7	3	3
GON	2	4	8	15	7	5	1
GOR	2	3	8	17	7	3	2
JIM	2	5	7	14	8	5	1
LAL	2	3	9	14	8	3	3
MKL	2	3	9	12	10	5	1
MTH	2	3	7	17	6	4	3
NKM	2	3	7	17	6	5	2
Total	30	53	95	237	88	57	28
Real Probability	5.1%	9.0%	16.1%	40.3%	15.0%	9.7%	4.8%

Note: AA, Addis Ababa; AW, Awassa; BDR, Bahirdar; COB, Combolcha; DD, Diredawa; DM, Debremarkos; DZ, Debrezite; GON, Gondar; GOR, Gore; JIM,Jima; LAL, Lalibela; MKL, Mkelle; MTH, Metehara; NKM, Nekemte

Table 3. JJAS regional drought and flood years in Ethiopia (1981-2022) using China Z index.

Grades	IF-ID	Flood/drought year	Total	Real probability
Extreme Flood	≥10	1988, 2020	2	4.8%
Severe Flood	[6.67, 10)	1996, 1998, 2007, 2019	4	9.5%

Continued

Mild Flood	(2.5, 6.67)	1994, 2001, 2006, 2010, 2011, 2012, 2021, 2022	8	19%
Normal	[−2.5, 2.5]	1981, 1986, 1989, 1990, 1991, 1992, 1993, 1999, 2000, 2003, 2005, 2008, 2013, 2016, 2017, 2018	16	38.1%
Mild Drought	(−6.67, −2.5)	1983, 1985, 1995, 2002, 2004, 2014	6	14.3%
Severe Drought	(−10, −6.67]	1984, 1997, 2009	3	7.1%
Extreme Drought	≤−10	1982, 1987, 2015	3	7.1%

3.4. Spatial Rainfall Distribution of Floods/Droughts

Based on the China Z index result presented in (Table 3) flood years (1988, 1996, 1998, 2007, 2019, and 2020) and the drought years (1982, 1984, 1987, 1997, 2009, and 2015) were selected for composite analysis. Spatial composite rainfall anomaly over Ethiopia during the JJAS (June-July-August-September) season is demonstrated in Figure 4, which indicates distinct patterns for such extreme events. During flood years, in most parts of Ethiopia, including the northeast, northern Somali region, Dire Dawa, Harari, Tigray, Amhara, western and central Oromia, Addis Ababa, Benishangul-Gumuz, Gambella, southwest, and most areas of the southern Region Figure 4(a), experienced above-average rainfall anomalies. These regions are vulnerable to flooding, considering that high rainfall amounts typically enhance flood risk. On the contrary, during drought periods, i.e., Figure 4(b), the rainfall deficit and rainfall below the average amount were recorded and resulted in the severe drought of the JJAS seasonal rainfall benefiting parts of the country. The drought is particularly damaging the northeast and eastern parts of the country, regions that are historically at risk of a prolonged dry spell, as noted by previous studies (Kebede et al., 2006; Seleshi & Zanke, 2004). The trends indicated Ethiopia's climate vulnerability to extreme rainfall events, which have significant impacts on agriculture, water resources, and food security (Alemayehu & Bewket, 2017). The findings emphasize the role of climate drivers like the Inter-Tropical Convergence Zone (ITCZ) and El Niño-Southern Oscillation (ENSO), which have been linked with Ethiopian rainfall variability and extreme events (Diro et al., 2011; Gissila et al., 2004; Korecha & Barnston, 2007; Segele et al., 2009).

3.5. Wind Anomaly Patterns

Figure 5 shows the anomaly wind circulation patterns in wet and dry years over Ethiopia, unveiling the country's atmospheric dynamics governing rainfall variability.

Figure 5(a) shows 850 hPa wind anomalies in Wet years throughout wet eras. Ethiopia qualifies as dominantly westerly wind anomalies, especially exceeding western and central Ethiopia. The current circulation is associated with increased moisture transport in the Atlantic Ocean and the Congo Basin, significantly contributing to above-average rainfall. Low-level convergence detects when these periods encourage vertical stretching, upward motion, and improved convection, which in turn creates favorable condition (Korecha & Barnston, 2007; Segele et

al., 2009). This strong flow of moisture with the positive vertical structure plays an important role in the development of thunderstorms in most parts of the country.

Figure 5(b) shows 850 hPa wind anomalies during dry years. In contrast, during dry years, the 850 hPa wind anomaly shifts to predominantly easterly flow, particularly over the eastern and southeastern regions of Ethiopia. That atmospheric shape is associated with decreased humidity and increased suppressed rainfall. The dominant easterly wind, which originates in the Indian Ocean and the Arabian Sea, is responsible for moisture depletion, thus suppressing rain and promoting dry conditions throughout the entire nation. This finding is consistent with the findings of (Korecha & Barnston, 2007; Segele et al., 2009; Viste & Sorteberg, 2013), which record easterly wind-decreased moisture and rainfall during a summer month. **Figure 5(c)** shows 200 hPa wind anomalies in wet periods by the upper atmosphere stage of 200 hPa. Ethiopia experiences a strengthening easterly wind anomaly during wet periods. The current enhanced easterly flow may indicate a well-developed Tropical Easterly Jet (TEJ), at 15˚ N a major influence on the Ethiopian summer monsoon. The intensification of the TEJ favors divergence forms on the upper levels, which in turn enhances low-level convergence and facilitates deep convection. During the JJAS period, this atmospheric configuration was significant for atmospheric convection and precipitation in Ethiopia (Diro et al., 2015). The interaction between the high and low levels of divergence and the convergence of the moisture content of the air above the region is responsible for the large amount of rainfall in the region. In **Figure 5(d)**, during Dry Seasons, 200 hPa wind anomalies are characterized by Westerly flow, which suppresses convection and reduces rainfall. The westerly anomaly, together with the low-level divergence, suppresses vertical movements and restricts the upward movement of moisture. Changes high-level circulation leads to suppressing rain over Ethiopia. The decreased high-level divergence (TEJ) and decreased convective task contribute to decreased precipitation formation during dry periods

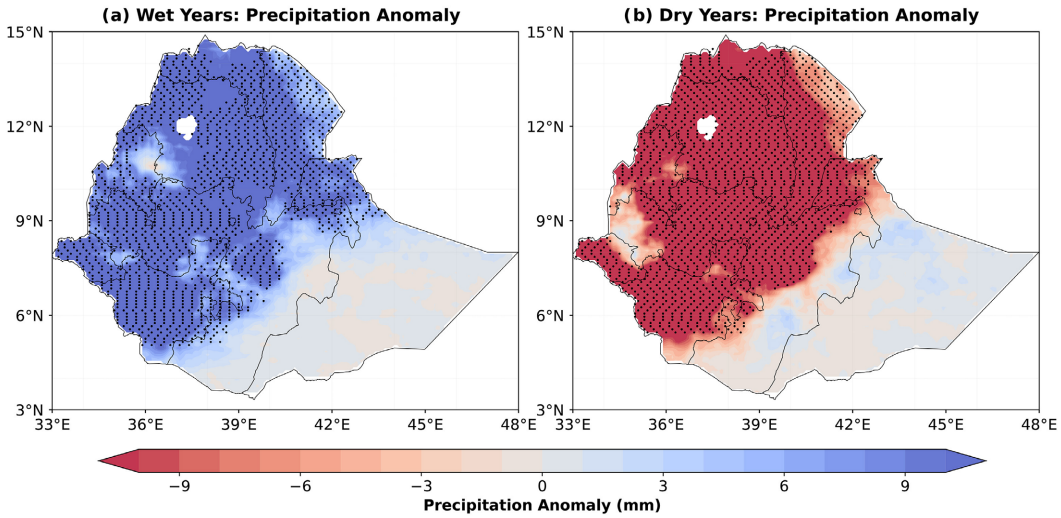

Figure 4. Composite Circulation Anomaly Patterns linked to Dry and Wet rainfall events during the JJAS season for Wet Years (a), and Dry Years (b). Black stipulated dotes represent significance at a 95% confidence level.

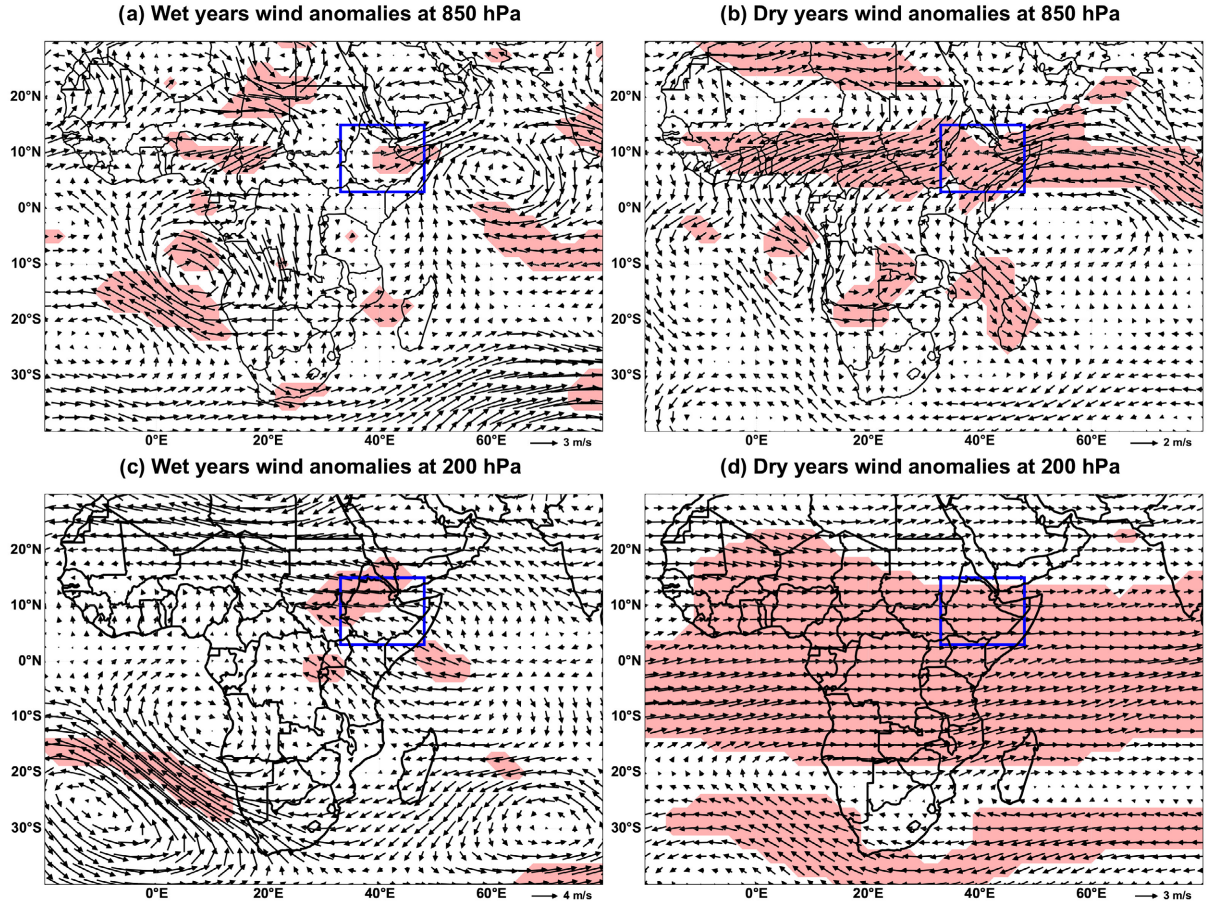

Figure 5. Composite wind anomaly vectors (ms^{-1}) for; wet years at (a) 850 hPa; (c) 200 hPa; dry years at (b) 850 hpa; (d) 200 hPa. Shaded are significant areas under statistical tests at 0.05 levels.

over Ethiopia. Diro et al. (2015) and Mulualem Abera & Wen (2021) have similarly noted the importance of low-level convergence and upper-level divergence during wet years, as well as the reverse pattern during dry years.

3.6. Velocity Potential/Divergent Wind Anomaly Pattern

Figures 6(a)-(d) illustrate the anomalous velocity potential and associated convergence/divergence patterns during composite wet and dry periods during the JJAS (June-July-August-September). These patterns reveal a distinct difference in atmospheric circulation between wet and dry periods, which plays a significant role in modulated rain beyond Ethiopia.

As shown in **Figure 6(a)**, wet years are distinguished by strong convergence close to the 850 hPa stage, particularly over the western Indian Ocean and the study area. This convergence facilitates upward movements and moisture accumulation, promoting rainfall in Ethiopia. At the same time, **Figure 6(c)** shows a divergence at the upper 200 hPa pressure level over Ethiopia and the Western Indian Ocean, which supports the rising motion of the lower levels. This coupling of low-level convergence and high-level divergence enhances convection and enhances a favorable state of precipitation, a finding consistent with previous inves-

tigations (Segele et al., 2009; Diro et al., 2015).

Dry years, in contrast, **Figure 6(b)**, and **Figure 6(d)** illustrate the circulation pattern during dry periods. At the 850 hPa level **Figure 6(b)**, divergence can be detected over Ethiopia, and the Western Indian Ocean, which reduces moisture convergence and upward movement. The present divergence at a lower level causes subsidence mainly due to the dry conditions. In parallel to the same span, **Figure 6(d)**, shows convergence at the upper level of 200 hPa, strengthening the downward motion and suppressing the convection, resulting in a significantly reduced rainfall. These findings coincide with the work of Viste & Sorteberg (2013) and Mulualem Abera & Wen (2021) which documented a similar atmospheric anomaly during dry years.

The rate of potential anomalies detected in **Figure 6(b)** is more clearly highlighted during dry periods compared to wet years. At a lower 850 hPa, the divergence over the western and eastern Indian Oceans is connected with convergence over the key equatorial central and eastern Pacific Ocean, which disrupts the transport of moisture essential for rain. Besides the 200 hPa pressure level, **Figure 6(d)** shows divergence over the central and eastern Pacific Ocean and convergence over Ethiopia and the Indian Oceans in the upper level. Such a pattern indicates a Walker-Cell response, with an upward motion anomaly over the warm sea surface temperature (SST) in the central and eastern Pacific Ocean and a reverse downward anomaly over the Indian Ocean.

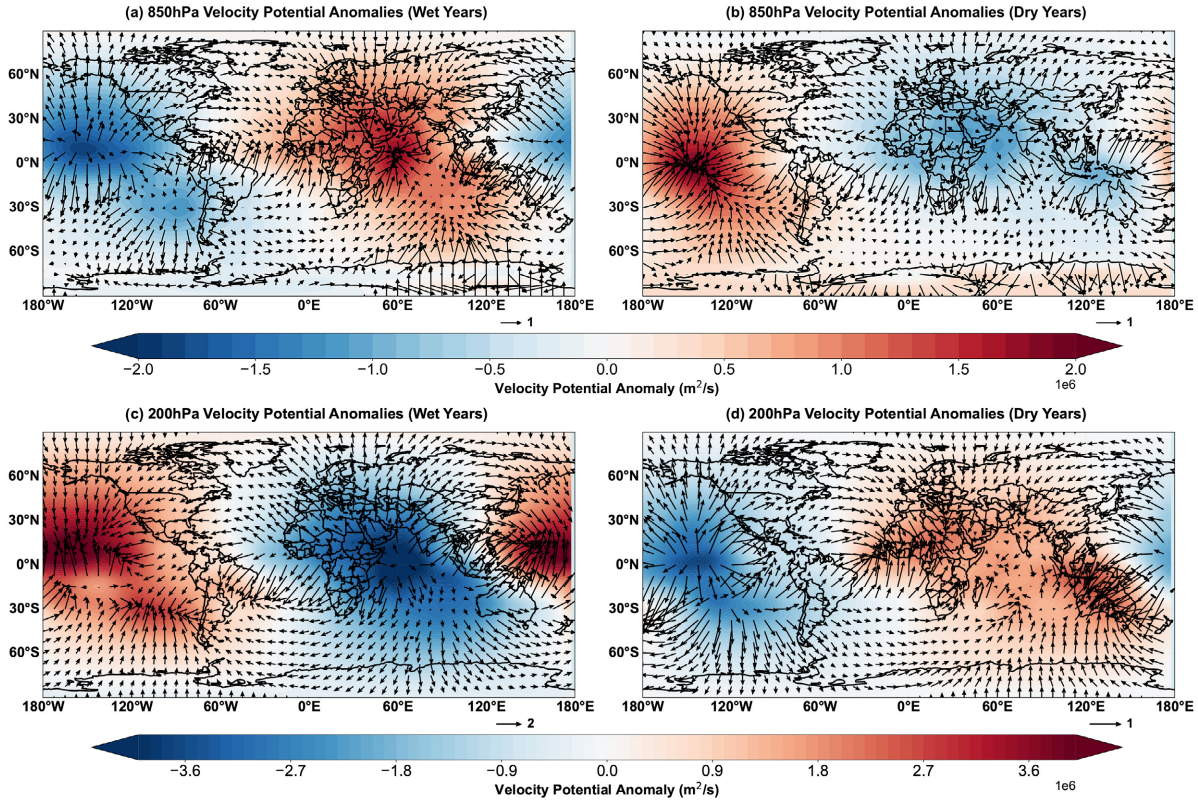

Figure 6. Composite anomaly of velocity potential (×106 m^2/s)/divergence (convergence) for wet years (a) 850 hPa and (c) 200 hPa; for dry years (b) 850 hPa and (d) 200 hPa. The red (blue) color indicates (convergent/divergent) ascending/descending) motion.

3.7. Vertical Velocity Anomaly Pattern

Figure 7(a) shows that during wet years, negative vertical velocity anomalies at approximately 3˚ - 15˚ N latitude and a fixed longitude of 40˚ E from 700 hPa - 200 hPa, indicate strong upward motion of convective air masses, mainly over western, southwestern, and northern parts of Ethiopia. This rising motion observed during wet years is dynamically supported by positive vorticity advection (PVA) throughout the atmospheric column. As low level PVA enhances cyclonic rotation, favors for low-level moisture convergence, and convective atmospheric instability, fostering deep convection and substantial rainfall over Ethiopia. Figure 7(b), in contrast, shows that during dry years, positive vertical velocity anomalies over northern and southwestern of the country indicate subsidence motion from 700 hPa to 200 hPa. This sinking motion promotes the formation of a high-pressure system or ridge through adiabatic warming, enhancing negative vorticity advection (NVA), which further stabilizes the atmosphere, suppresses convection, and limits moisture accumulation, inhibits cloud formation and precipitation (Holton & Hakim, 2013). Vorticity advection, a crucial factor in modulating vertical motion and precipitation patterns, plays a crucial role in governing convection for JJAS season. For instance, positive vorticity advection (PVA) in the upper and middle levels strengthens the upward motion, promoting deep convection and increased rainfall, while negative vorticity advection (NVA) is associated with subsidence and suppression of convection (Holton & Hakim, 2013). The difference between wet and dry years emphasizes the crucial role of vertical motion in regulating Ethiopia's precipitation. While descending motion during dry periods causes moisture deficits and drought conditions over the study area, ascending motion during wetter periods enhances convection and promotes rainfall.

3.8. Outgoing Longwave Radiation Anomaly Pattern

Figure 8 presents a composite pattern of Longwave Radiation (OLR) in Ethiopia during the June-September (JJAS) period, distinguishing between the wet years and the dry years. The OLR is a key indicator for cloud enhancement and convective activity and provides essential information on the atmospheric condition associated with the seasonal variations of Ethiopian rainfall. Figure 8(a), that the OLR in Ethiopia is significantly negative (−15 to −20 W/m^2), especially in the western, central, and northern parts of the country during wet years. These decreased values of OLR indicate by implying increased cloud formation and convective instability of the atmosphere, which strongly correlates with increased rainfall during the JJAS period over most parts of Ethiopia. The lowest OLR anomalies −20 W/m^2, are dominantly over the western Highlands, suggesting strong convection and widespread rainfall in the above-mentioned areas. The spatial distribution of the OLR is consistent with the precipitation pattern of Ethiopia, where the western, central, northwestern eastern, and southwestern parts of the country usually receive heavy rain during the summer monsoon. The negative OLR anomaly in the abovementioned areas confirms the vital role of enhanced atmospheric instability in driving precipitation during wet years. Figure 8(b), in

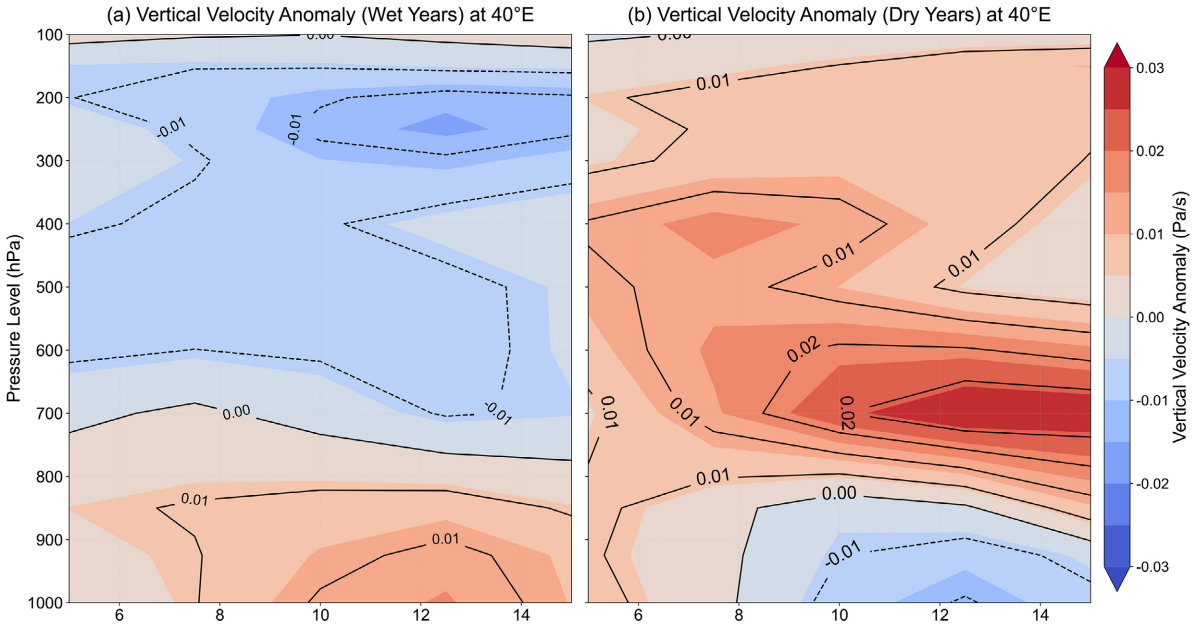

Figure 7. Vertical Velocity Anomalies; wet years (a) and dry years (b) at a fixed longitude 40˚ E. The red/blue significant/insignificant area. The Brocken (Solid) lines show ascending (descending) motion. Negative (positive) values indicate upward (downward) motion. The contour interval is 0.01 and units are in Pa/s.

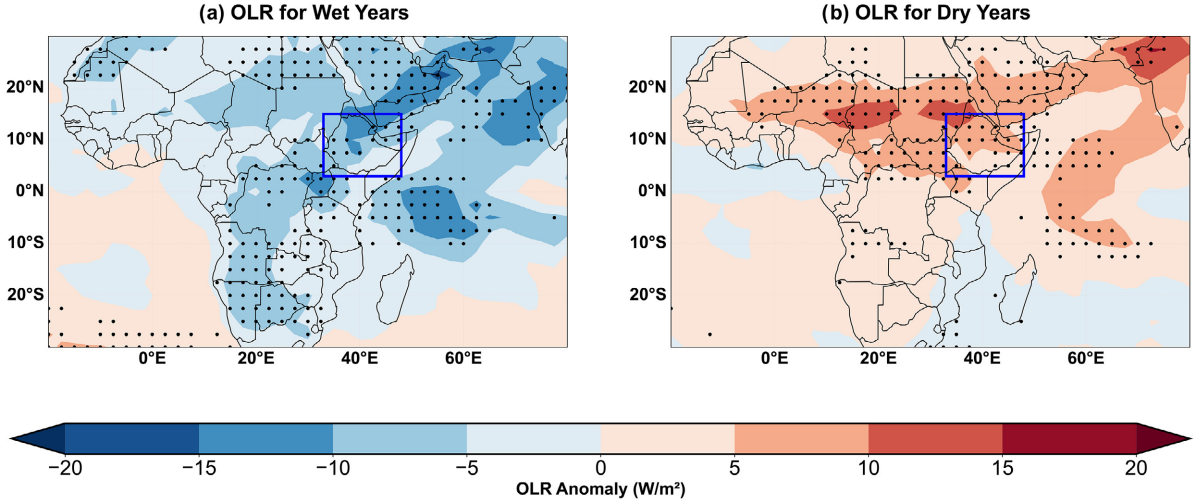

Figure 8. The OLR (W/m^2) (a) for wet years and (b) for dry years. Black stipulated dots represent significance at a 0.05 confidence level.

contrast, dry years in Ethiopia show significantly positive (5 - 10 W/m^2) OLR anomalies, with a decrease in cloud formation and reduced convective systems. High OLR values, exceeding 10 W/m^2 in central, west, northwest, east, and northeast parts of the country, due to suppressed convection and decreased rainfall. The above-mentioned higher OLR anomalies highlight atmospheric stability and the lack of substantial moisture convergence during dry years. The results are consistent with those of (Mulualem Abera & Wen, 2021). The striking difference in OLR during the period of wet and dry periods highlights the impact of atmos-

pheric instability on rain variability and emphasizes the role of convective cloud formation in regulating Ethiopia's seasonal rainfall.

3.9. Relative Humidity

Figure 9 shows the spatial distribution of relative humidity (RH) at 850 hPa in Ethiopia during the June-September (JJAS) period, comparing the composites of the wet and dry years. The role of atmospheric moisture in shaping seasonal variations in rainfall over the region. Figure 9(a) shows increased RH during moisture seasons in central, western, northwestern, southern, southwestern, and eastern Ethiopia. In these areas, the relative humidity is increased by approximately (4% - 9%), a remarkable indicator of increased atmospheric moisture availability. Higher relative humidity is favorable for cloud formation and precipitation, especially during the monsoon months of July and August, when the rain is usually more intense. In addition to the increase in rainfall, the increased moisture availability is mainly due to the northward passage of the Inter-Tropical Convergence Zone (ITCZ), which facilitates the convection of moist air in most parts of the country. The higher RH values are consistent with the moist atmosphere characteristic of wet years, which contribute to the formation of convective atmospheric instability and extreme rainfall in the highlands of Ethiopia. In contrast, dry years in Ethiopia have significant negative RH anomaly (−5% to −9%) mainly over the northwestern, eastern, central, southwest, and southern highlands regions. These negative anomalies indicate the reduction in atmospheric moisture associated with subsidence and the downward motion in the atmosphere. Such conditions reduce cloud formation and precipitation, resulting in drier conditions in most parts of the country. The northern and northeastern regions are experiencing a worsening moisture deficit during dry years, becoming increasingly arid. Furthermore, the stable atmospheric condition is further hindered by the significant moisture deficit during dry periods, thereby contributing to the continuity of drought conditions in the region's seasonal rainfall.

3.10. Sea Surface Temperature Anomaly Pattern

Figure 10 compares moisture conditions and dry periods in Ethiopia using the composite sea surface temperature (SSTs) during the June-September (JJAS) period. Figure 10(a) shows a cooler-than-average sea surface temperature in the central and eastern equatorial Pacific indicating La Niña conditions. The Indian ocean SSTs are warm, particularly in the western Indian ocean, and also warm SSTs over western Pacific Ocean. During JJAS wet years, these warm SST anomalies help facilitate moisture transport from the Indian and Pacific Oceans to enhance rainfall in Ethiopia. The cooler central and eastern Pacific sea surface temperature, together with the warming of the Indian Ocean and the favorable atmospheric conditions for precipitation, support the positive feedback mechanism that increases the monsoonal rainfall in Ethiopia. Figure 10(b) shows that, during dry years, warmer-than-normal SSTs can be detected in the central, and eastern equatorial Pacific, suggesting that El Nino-like event. Such situations are usually associated with a different pat-

tern of SST in the Indian Ocean together with a warmer anomaly in the West Indian Ocean, and cooler SST in the western Pacific Ocean. The presence of El Niño conditions disrupts normal atmospheric circulation patterns, principally reducing moisture transport and suppressing rainfall over Ethiopia. The warmer Pacific SSTs, together with a changed wind shape, suppress convection in the study area, thereby promoting drought and moisture deficiency. This finding aligns with several previous studies (Diro et al., 2011; Mulualem Abera & Wen, 2021; Segele et al., 2009).

3.11. Correlation Analysis

Figure 11 illustrates the correlation between Ethiopian June-September (JJAS) rainfall, global sea surface temperatures (SSTs), and the Niño 3.4 index. Figure 11(a), the correlation pattern shows significant negative (−0.8) values in the central and eastern equatorial Pacific, indicating that cooler SSTs in this region are associated with increased rainfall over Ethiopia during JJAS. A significant

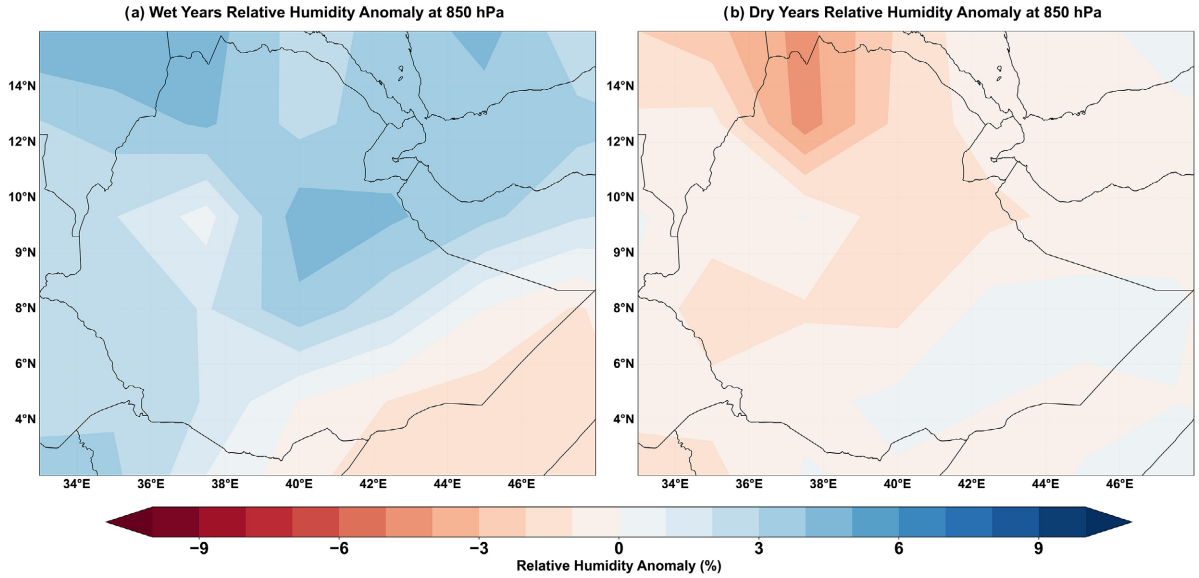

Figure 9. The Relative Humidity (in %) (a) For wet years at 850 hPa, and (b) For dry years at 850 hPa.

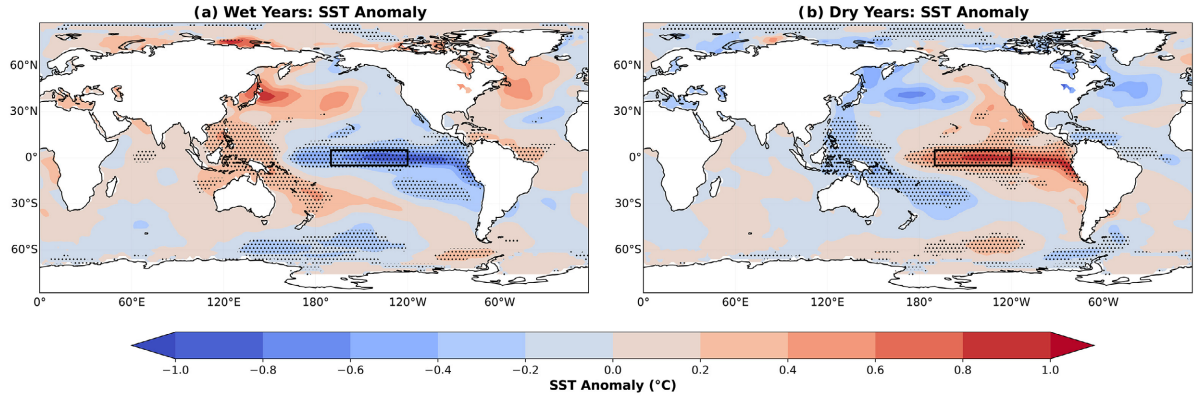

Figure 10. Composite SST (shading; ˚C) anomaly pattern for wet years (a), and (b) for dry years. Black Stipulated Dots represent areas statistically significant at a 0.05 confidence level.

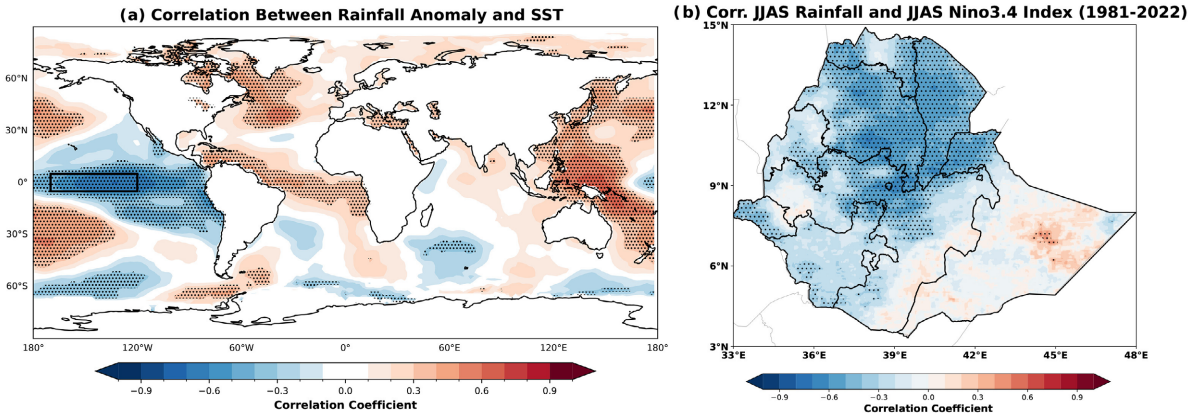

Figure 11. JJAS Ethiopian rainfall correlation with June SST for the regions of (a) Correlation between JJAS seasonal rainfall and SST (a), and (b) JJAS seasonal Rainfall and Nino 3.4 Index. Black Dots Stipulated represent significance at a 95% confidence level.

positive (0.8) correlation has been detected in the western Pacific Ocean, suggesting that warmer SSTs in these areas correspond to increased Ethiopian rainfall. Suggesting that warmer SSTs in these areas correspond to enhanced Ethiopian rainfall. These findings are in line with the work of (Korecha & Barnston, 2007) who examined the same spatial patterns in the ENSO-rainfall relationship over Ethiopia. **Figure 11(b)**, the correlation map shows a predominantly significant negative relationship in major parts of Ethiopia, especially robust in the northern half of the country, central, eastern, southern highlands, and southwest areas. In the northeast, central and eastern parts of the country, the correlation coefficient ranged from −0.4 to −0.8. This indicated that the positive values of the Nino 3.4 Index (El Nino conditions) are associated with decreased rainfall in Ethiopia for JJAS, while the negative SST in the Nino 3.4 Index (La Nina conditions) corresponds to increased rainfall. With the Nino 3.4 index, the southeast lowlands show a weaker positive correlation. This finding is in agreement with the work of (Diro et al., 2011; Segele et al., 2009), who indicated similar spatial patterns for the ENSO-rainfall relationship in Ethiopia. Such relationships indicate the significant impact of ENSO on Ethiopian JJAS rainfall variability and provide evidence of the potential application of SST patterns, especially the Nino 3.4 Index, to predict seasonal rainfall in Ethiopia (Gissila et al., 2004).

4. Summary and Conclusion

The present analysis uses the China Z-index probability to measure the frequency and severity of floods and droughts in Ethiopia during the June-September (JJAS) period from 1981-2022. The analysis of flood and drought probabilities shows consistency between observed/calculated and theoretical distributions. Normal rainfall conditions accounted for 40.3%, while dry and wet conditions represented 29.5% and 30.2%, respectively. Extreme floods were observed in 1988 and 2020, with severe events in 1996, 1998, 2007, and 2019. Conversely, extreme droughts occurred in 1982, 1987, and 2015, while 1984, 1997, and 2009 experienced severe

droughts. Over 42 years, 14 wet years and 12 dry years were recorded, with dry events dominating before 1998 and wet events increasing thereafter. Regional rainfall anomalies during these events show distinct patterns; flood years had increased rainfall in most parts of the country, while drought years had a significant rainfall deficit, particularly in the northeast and eastern regions of Ethiopia. The results show the relevance of wind circulation at different pressure levels to Ethiopian rainfall. During the wet years, the westerly wind, at 850 hPa, and the easterly wind, at 200 hPa, facilitated to transport of moisture and increased convection, driving rain. Similarly, dry years were associated with an easterly wind accompanying 850 hPa and a westerly wind near 200 hPa, which suppressed moisture and reduced convection over the study area. In addition to analyzing the effects of sea surface temperature (SST) anomalies on Ethiopian rainfall, especially in the Pacific and Indian Oceans. The cooler-than-average SSTs in the central and eastern Pacific and warm SSTs in the Indian Ocean enhanced moisture transport, mainly promoting increased rainfall. In contrast, warmer-than-normal SSTs in the central and eastern Pacific, as seen during the El Nino event, reduce moisture transport and result in deficit rainfall over Ethiopia in the JJAS season. JJAS Ethiopian seasonal rainfall and the Nino 3.4 Index, a strong negative (−0.8) relationship was detected, implying that La Nina conditions were associated with increased rainfall, while El Nino conditions were led to suppress rainfall. The analysis of longwave radiation (OLR) and relative humidity (RH) anomalies further confirms these conditions, with wet years presenting negative OLR anomalies and increased RH, indicating improved cloud formation and precipitation, while dry years exhibit positive OLR anomalies and decreased RH, implying suppression of atmospheric convection. These findings offer valuable insights into the major climate drivers affecting Ethiopia's rainfall variability, which may help to improve seasonal rainfall forecasting and adaptation plans.

While this study provides good understanding of large-scale atmospheric and oceanic drivers of Ethiopian JJAS rainfall variability, it has some limitations that require further study. Future research efforts will include high-resolution regional climate models (RCMs) and denser observational networks (e.g., satellite-derived rainfall estimates, automatic weather stations) to better represent the mesoscale convective systems, land-atmosphere interactions, and local circulation patterns, and thereby improve the resolution of spatial rainfall variability. Also, exploring the role of aerosols, and microphysical processes in modifying convection is important. The use of advanced statistical techniques along with Artificial Intelligence (AI) and Machine Learning (ML) could help in understanding circulation anomalies, and improve season rainfall prediction and assessments of climate risk for extreme events in Ethiopia.

Author Contributions

Habtamu Tarekegn Negash: Conceptualization, methodology, data collection, formal analysis, investigation, validation, visualization, writing-original draft, re-

view & editing.

Mulualem Abera Waza: Conceptualization, methodology, visualization review & editing. All authors made significant contributions to the study, reviewed the manuscript, and approved the final version for submission.

Acknowledgments

The authors would like to express sincere gratitude to the Climate Hazards Group Infrared Precipitation with Station (CHIRPS), NOAA/NCDC, NOAA/NCEP-NCAR, and the Ethiopian Meteorological Institute (EMI) for providing the datasets used in this study. The first author would like to express special thanks to the Ministry of Commerce, People's Republic of China (MOFCOM) for sponsoring my study in China, and to Nanjing University of Information Science and Technology for providing an enabling work environment and the necessary facilities for data analysis. The first author is deeply grateful to Prof. Guangxin He for his supervision and invaluable guidance, and to Prof. Tan Guirong for the insightful advice and support provided during the research period.

Data Availability Statement

The datasets used in this study include both publicly accessible and restricted data. Open-source datasets from CHIRPS, NOAA/NCDC, and NOAA/NCEP-NCAR are freely available through their respective websites.

CHIRPS:
https://data.chc.ucsb.edu/products/CHIRPS-2.0/global_monthly/netcdf/.

Monthly Extended Reconstructed SST Version 5:
https://iridl.ldeo.columbia.edu/SOURCES/.NOAA/.NCDC/.ERSST/.version5/.sst/,
the National Centers for Environmental Prediction/National Center for Atmospheric Research, websites:
https://iridl.ldeo.columbia.edu/SOURCES/.NOAA/.NCEP-NCAR/.CDAS-1/.MONTHLY/.Intrinsic/.PressureLevel/, and National Oceanic and Atmospheric Administration (NOAA) Physical Science Laboratory (PSL) websites:
https://psl.noaa.gov/data/gridded/data.olrcdr.interp.html. However, observational data from the Ethiopian Meteorological Institute (EMI) are not much and cannot be shared due to institution policies.

Conflicts of Interest

The authors declare no conflicts of interest regarding the publication of this paper.

References

Abdi, A. M., Vrieling, A., Yengoh, G. T., Anyamba, A., Seaquist, J. W., Ummenhofer, C. C. et al. (2016). The El Niño—La Niña Cycle and Recent Trends in Supply and Demand of Net Primary Productivity in African Drylands. *Climatic Change, 138,* 111-125. https://doi.org/10.1007/s10584-016-1730-1

Alemayehu, A., & Bewket, W. (2017). Local Spatiotemporal Variability and Trends in Rainfall and Temperature in the Central Highlands of Ethiopia. *Geografiska Annaler: Series*

A, Physical Geography, 99, 85-101. https://doi.org/10.1080/04353676.2017.1289460

Alexander, F., & Nyasulu, M. (2021). Diagnosis of Wet and Dry Events and Its Associated Atmospheric Circulation Anomaly over Malawi, Southeast Africa. *Dynamics of Atmospheres and Oceans, 94,* Article ID: 101221. https://doi.org/10.1016/j.dynatmoce.2021.101221

Alhamshry, A., Fenta, A. A., Yasuda, H., Kimura, R., & Shimizu, K. (2019). Seasonal Rainfall Variability in Ethiopia and Its Long-Term Link to Global Sea Surface Temperatures. *Water, 12,* Article No. 55. https://doi.org/10.3390/w12010055

Ayehu, G. T., Tadesse, T., Gessesse, B., & Dinku, T. (2018). Validation of New Satellite Rainfall Products over the Upper Blue Nile Basin, Ethiopia. *Atmospheric Measurement Techniques, 11,* 1921-1936. https://doi.org/10.5194/amt-11-1921-2018

Berihu, T., Chen, W., & Wang, L. (2024). Rainfall Variability and Its Teleconnection with Atmospheric Circulation Anomalies over Southern and Southeastern Region, Ethiopia. *Theoretical and Applied Climatology, 155,* 5819-5834. https://doi.org/10.1007/s00704-024-04956-0

Bewket, W., & Conway, D. (2007). A Note on the Temporal and Spatial Variability of Rainfall in the Drought-prone Amhara Region of Ethiopia. *International Journal of Climatology, 27,* 1467-1477. https://doi.org/10.1002/joc.1481

Cheung, W. H., Senay, G. B., & Singh, A. (2008). Trends and Spatial Distribution of Annual and Seasonal Rainfall in Ethiopia. *International Journal of Climatology, 28,* 1723-1734. https://doi.org/10.1002/joc.1623

CIAT, BFS/USAID (2017). *Climate-Smart Agriculture in Ethiopia. CSA Country Profiles for Africa Series* (26 p.). International Center for Tropical Agriculture (CIAT); Bureau for Food Security, United States Agency for International Development (BFS/USAID).

Climate Risk Profile (n.d.). *Ethiopia (2021)*. The World Bank Group.

Conway, D. (2000). The Climate and Hydrology of the Upper Blue Nile River. *The Geographical Journal, 166,* 49-62. https://doi.org/10.1111/j.1475-4959.2000.tb00006.x

Conway, D., & Schipper, E. L. F. (2011). Adaptation to Climate Change in Africa: Challenges and Opportunities Identified from Ethiopia. *Global Environmental Change, 21,* 227-237. https://doi.org/10.1016/j.gloenvcha.2010.07.013

Dai, A. (2011). Drought under Global Warming: A Review. *WIREs Climate Change, 2,* 45-65. https://doi.org/10.1002/wcc.81

Degefu, M. A., Rowell, D. P., & Bewket, W. (2017). Teleconnections between Ethiopian Rainfall Variability and Global SSTs: Observations and Methods for Model Evaluation. *Meteorology and Atmospheric Physics, 129,* 173-186. https://doi.org/10.1007/s00703-016-0466-9

Deressa, T. T., Hassan, R. M., Ringler, C., Alemu, T., & Yesuf, M. (2009). Determinants of Farmers' Choice of Adaptation Methods to Climate Change in the Nile Basin of Ethiopia. *Global Environmental Change, 19,* 248-255. https://doi.org/10.1016/j.gloenvcha.2009.01.002

Diao, X., Ellis, M., Pauw, K., & Thurlow, J. (2023). *Ethiopia's Agrifood System Structure and Drivers of Transformation*.

Dinku, T., Funk, C., Peterson, P., Maidment, R., Tadesse, T., Gadain, H. et al. (2018). Validation of the CHIRPS Satellite Rainfall Estimates over Eastern Africa. *Quarterly Journal of the Royal Meteorological Society, 144,* 292-312. https://doi.org/10.1002/qj.3244

Diro, G. T., Grimes, D. I. F., & Black, E. (2011). Teleconnections between Ethiopian Summer Rainfall and Sea Surface Temperature: Part I—Observation and Modelling. *Climate Dynamics, 37,* 103-119. https://doi.org/10.1007/s00382-010-0837-8

Diro, G. T., Grimes, D. I. F., & Black, E. (2015). Large Scale Features Affecting Ethiopian Rainfall. In C. J. R. Williams, & D. R. Kniveton (Eds.), *Advances in Global Change Research* (pp. 13-50). Springer. https://doi.org/10.1007/978-90-481-3842-5_2

Dogan, S., Berktay, A., & Singh, V. P. (2012). Comparison of Multi-Monthly Rainfall-Based Drought Severity Indices, with Application to Semi-Arid Konya Closed Basin, Turkey. *Journal of Hydrology, 470,* 255-268. https://doi.org/10.1016/j.jhydrol.2012.09.003

Dong, J., Xing, L., Cui, N., Zhao, L., Guo, L., & Gong, D. (2023). Standardized Precipitation Evapotranspiration Index (SPEI) Estimated Using Variant Long Short-Term Memory Network at Four Climatic Zones of China. *Computers and Electronics in Agriculture, 213,* Article ID: 108253. https://doi.org/10.1016/j.compag.2023.108253

FAO (2016). *AQUASTAT Country Profile—Ethiopia*. Food and Agriculture Organization of the United Nations (FAO).

Folland, C. K. (1983). Regional-Scale Interannual Variability of Climate. A Northwest European Perspective. *Meteorological Magazine, 112,* 163-183.

Funk, C., Peterson, P., Landsfeld, M., Pedreros, D., Verdin, J., Shukla, S. et al. (2015). The Climate Hazards Infrared Precipitation with Stations—A New Environmental Record for Monitoring Extremes. *Scientific Data, 2,* Article ID: 150066. https://doi.org/10.1038/sdata.2015.66

Gamachu, D. (1988). Some Patterns of Altitudinal Variation of Climatic Elements in the Mountainous Regions of Ethiopia. *Mountain Research and Development, 8,* Article No. 131. https://doi.org/10.2307/3673439

Gissila, T., Black, E., Grimes, D. I. F., & Slingo, J. M. (2004). Seasonal Forecasting of the Ethiopian Summer Rains. *International Journal of Climatology, 24,* 1345-1358. https://doi.org/10.1002/joc.1078

Gobie, B. G., & Miheretu, B. A. (2021). Effects of El Nino Southern Oscillation Events on Rainfall Variability over Northeast Ethiopia. *Modeling Earth Systems and Environment, 7,* 2733-2739. https://doi.org/10.1007/s40808-020-01060-w

Gummadi, S., Rao, K. P. C., Seid, J., Legesse, G., Kadiyala, M. D. M., Takele, R. et al. (2017). Spatio-Temporal Variability and Trends of Precipitation and Extreme Rainfall Events in Ethiopia in 1980-2010. *Theoretical and Applied Climatology, 134,* 1315-1328. https://doi.org/10.1007/s00704-017-2340-1

Holton, J. R., & Hakim, G. J. (2013). *An Introduction to Dynamic Meteorology* (p. 88). Academic Press.

Huang, B., Thorne, P. W., Banzon, V. F., Boyer, T., Chepurin, G., Lawrimore, J. H. et al. (2017). Extended Reconstructed Sea Surface Temperature, Version 5 (ERSSTv5): Upgrades, Validations, and Intercomparisons. *Journal of Climate, 30,* 8179-8205. https://doi.org/10.1175/jcli-d-16-0836.1

Jury, M. R., & Funk, C. (2013). Climatic Trends over Ethiopia: Regional Signals and Drivers. *International Journal of Climatology, 33,* 1924-1935. https://doi.org/10.1002/joc.3560

Kalnay, E., Kanamitsu, M., Kistler, R., Collins, W., Deaven, D., Gandin, L. et al. (1996). The NCEP/NCAR 40-Year Reanalysis Project. *Bulletin of the American Meteorological Society, 77,* 437-471. https://doi.org/10.1175/1520-0477(1996)077<0437:tnyrp>2.0.co;2

Kassahun, B. (1987). Weather Systems over Ethiopia. In *Proceedings of 1st Tech Conference on Meteorological Research in Eastern and Southern Africa* (pp. 53-57). UCAR.

Kebede, S., Travi, Y., Alemayehu, T., & Marc, V. (2006). Water Balance of Lake Tana and Its Sensitivity to Fluctuations in Rainfall, Blue Nile Basin, Ethiopia. *Journal of Hydrology, 316,* 233-247. https://doi.org/10.1016/j.jhydrol.2005.05.011

Kistler, R., Collins, W., Saha, S., White, G., Woollen, J., Kalnay, E. et al. (2001). The NCEP-NCAR 50-Year Reanalysis: Monthly Means CD-ROM and Documentation. *Bulletin of the American Meteorological Society, 82,* 247-267. https://doi.org/10.1175/1520-0477(2001)082<0247:tnnyrm>2.3.co;2

Korecha, D., & Barnston, A. G. (2007). Predictability of June-September Rainfall in Ethiopia. *Monthly Weather Review, 135,* 628-650. https://doi.org/10.1175/mwr3304.1

Makula, E. K., & Zhou, B. (2021). Changes in March to May Rainfall over Tanzania during 1978-2017. *International Journal of Climatology, 41,* 5663-5675. https://doi.org/10.1002/joc.7146

MoEF (Ministry of Environment and Forest) (2015). *Ethiopia's Second National Communication to the United Nations Framework Convention on Climate Change (UNFCCC).* The Federal Democratic Republic of Ethiopia. https://unfccc.int/resource/docs/natc/ethnc2.pdf

Mulualem Abera, W., & Wen, W. (2021). Interannual Variability of Seasonal Rainfall and Associated Circulations over Gambella, Ethiopia. *International Journal of Environmental Monitoring and Analysis, 9,* Article No. 67. https://doi.org/10.11648/j.ijema.20210903.13

Ngoma, H., Wen, W., Ojara, M., & Ayugi, B. (2021). Assessing Current and Future Spatiotemporal Precipitation Variability and Trends over Uganda, East Africa, Based on CHIRPS and Regional Climate Model Datasets. *Meteorology and Atmospheric Physics, 133,* 823-843. https://doi.org/10.1007/s00703-021-00784-3

Nicholson, S. E. (2017). Climate and Climatic Variability of Rainfall over Eastern Africa. *Reviews of Geophysics, 55,* 590-635. https://doi.org/10.1002/2016rg000544

Nicholson, S. E. (2018). The ITCZ and the Seasonal Cycle over Equatorial Africa. *Bulletin of the American Meteorological Society, 99,* 337-348. https://doi.org/10.1175/bams-d-16-0287.1

OCHA (2024). *Ethiopia—Situation Report.* https://www.unocha.org/publications/report/ethiopia/ethiopia-situation-report-10-jan-2024

Ogwang, B. A., Guirong, T., & Haishan, C. (2012). Diagnosis of September-November Drought and the Associated Circulation Anomalies over Uganda. *Pakistan Journal of Meteorology, 9,* 11-24. http://www.pmd.gov.pk/rnd/rnd_files/vol8_issue17/2.pdf

Segele, Z. T., & Lamb, P. J. (2005). Characterization and Variability of Kiremt Rainy Season over Ethiopia. *Meteorology and Atmospheric Physics, 89,* 153-180. https://doi.org/10.1007/s00703-005-0127-x

Segele, Z. T., Lamb, P. J., & Leslie, L. M. (2009). Large-Scale Atmospheric Circulation and Global Sea Surface Temperature Associations with Horn of Africa June-September Rainfall. *International Journal of Climatology, 29,* 1075-1100. https://doi.org/10.1002/joc.1751

Seleshi, Y., & Zanke, U. (2004). Recent Changes in Rainfall and Rainy Days in Ethiopia. *International Journal of Climatology, 24,* 973-983. https://doi.org/10.1002/joc.1052

Suribabu, C. R., & Sujatha, E. R. (2019). Evaluation of Moisture Level Using Precipitation Indices as a Landslide Triggering Factor—A Study of Coonoor Hill Station. *Climate, 7,* Article No. 111. https://doi.org/10.3390/cli7090111

Tan, G., Sun, Z., & Chen, H. (2003). Diagnosis of Summertime Floods/Droughts and Their Atmospheric Circulation Anomalies over North China. *Acta Meteorologica Sinica (English Edition), No. 3,* 257–273.

UNISDR (2015). *The Human Cost of Weather-Related Disasters 1995-2015.*

https://www.unisdr.org/files/46796_cop21weatherdisastersreport2015.pdf

Viste, E., & Sorteberg, A. (2013). Moisture Transport into the Ethiopian Highlands. *International Journal of Climatology, 33,* 249-263. https://doi.org/10.1002/joc.3409

Von Storch, H., & Zwiers, F. W. (1984). *Statistical Analysis in Climate Research.* Cambridge University Press. https://doi.org/10.1017/CBO9780511612336

Wang, Z. W., Zhai, P. M., & Zhang, H. T. (2003). Variation of Drought over Northern China during 1950-2000. *Journal of Geographical Sciences, 13,* 480-487. https://doi.org/10.1007/bf02837887

Wilks, D. S. (2006). *Statistical Methods in the Atmospheric Sciences* (2nd ed.). Academic Press.

Wilks, D. S. (2011). *Statistical Methods in the Atmospheric Sciences* (p. 100). Academic Press.

World Bank Group (2024). *Ethiopia Country Climate and Development Report, February 2024. CCDR Series*. World Bank. http://hdl.handle.net/10986/41114

Wu, H., Hayes, M. J., Weiss, A., & Hu, Q. (2001). An Evaluation of the Standardized Precipitation Index, the China-Z Index and the Statistical Z-Score. *International Journal of Climatology, 21,* 745-758. https://doi.org/10.1002/joc.658